Energy 291 (2024) 130237

Contents lists available at ScienceDirect

Energy

journal homepage: www.elsevier.com/locate/energy

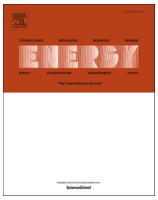

Quantifying effects of surface morphology and functional groups of carbon fibers on mass transfer coefficient in vanadium redox flow batteries

Menglian Zheng [a,b,c], Ke Liu [b,c], Jie Sun [d,*], Zitao Yu [b,c]

[a] Institute of Wenzhou, Zhejiang University, Wenzhou, 325036, China
[b] State Key Laboratory of Clean Energy Utilization, Hangzhou, 310027, China
[c] Institute of Thermal Science and Power Systems, Zhejiang University, Hangzhou, 310027, China
[d] Institute of Energy and Environment Engineering, NingboTech University, Ningbo, 315100, China

ARTICLE INFO

Handling editor: Dr. A. Olabi

Keywords:
Redox flow battery
Mass transfer coefficient
Surface morphology
Functional groups
Dimensionless correlations

ABSTRACT

Optimization of porous electrodes has emerged as a fascinating alternative to improve the power density of redox flow batteries. While numerous studies have demonstrated the significant reduction in overpotentials due to electrode modifications, there has yet to be research that elucidates the underlying mechanism. The developed fitting model in the present study enables efficient mass transfer coefficient characterization for redox flow battery systems with sluggish reactants. Based on the newly proposed fitting model and experimental data, the present study explores the mechanism of how changes in electrode morphology and functional groups affect the mass transfer coefficient. It is found that micro-scale pores on the fiber surface, when fibers were thermally treated at 300 °C, successfully enhanced mass transfer of the reactants in the electrode likely owing to the shortened diffusion distance, while nano-scale pores, when fibers thermally treated at 400 °C, showed minor effects on mass transfer enhancement. Besides, the increment of the oxygen containing functional groups also enhanced the mass transfer rate in the diffusion layer likely attributable to the improved electrode hydrophilicity. Last, the power-law correlations for Sherwood number and Reynolds number for different electrode samples were established, enabling frontend screening in future's electrode development campaigns.

1. Introduction

The intermittency of renewable power motivates the integration of efficient and cost-effective energy storage in advanced energy systems [1]. Research into new generation materials with the goal of reducing system costs of redox flow batteries (RFBs) is right in the hot spot (as reviewed in Refs. [2,3]).

Plenty of material preparation and treatments methods have been investigated over the last decades [4,5]. Like all other energy storage technologies, optimization of porous electrodes has emerged as a fascinating solution to improve the power density of RFBs and thus reduce the battery system costs [6,7]. Existing studies have experimentally verified that surface morphology and functional groups have obvious effects on the reaction and concentration overpotential of RFBs [8]: the changed surface morphology may increase the specific surface area, while the added functional groups can enhance the kinetic reactivity, both of which reduce the reaction overpotential significantly. For example, Zhou et al. significantly enhanced the energy efficiency for vanadium RFBs through dual-scale pores [9]. Fu et al. demonstrated the enhancement in the kinetics for vanadium RFBs by coating defect-rich graphene [10]. Abbas et al. and Li et al. showed the catalytic impacts of carbon nanorods [11] and multi-walled carbon nanotubes [12] for VO_2^+/VO^{2+} redox, respectively. However, to our best knowledge, no quantitative studies have been conducted on the effects of the surface morphology and surface functional groups on the mass transfer process of reactants, which determines the concentration overpotential in RFBs.

The measurements of the mass transfer coefficient of porous media traces back to 1980s [13–15], when Schmal et al. developed the dimensionless relations between Sherwood number and Reynold number for single carbon fiber, bundle of fibers, carbon paper, and carbon felt by using the most commonly used approach, i.e., the mass transfer dominant limiting current density method (MD method). Targeting the mass transfer problems in RFBs, You et al. [16] and Xu et al. [17] both utilized MD method for characterizing mass transfer coefficients for RFBs. It was emphasized that anolyte or catholyte should be diluted to make it the mass transfer limiting side [17]. Recognizing the importance

* Corresponding author.
E-mail address: 11627019@zju.edu.cn (J. Sun).

https://doi.org/10.1016/j.energy.2024.130237
Received 2 April 2023; Received in revised form 29 December 2023; Accepted 1 January 2024
Available online 4 January 2024

of flow fields on mass transfer [18], Milshtain et al. investigated the impacts of the applied flow field on the mass transfer coefficient [19]. Forner-Cuenca et al. [20] and Tenny et al. [21] employed the MD method to characterize the volumetric mass transfer capabilities among graphite felt, carbon paper, and carbon paper with varying weave patterns. In addition to the above characterization work, the MD method by itself has also been advanced. Recognizing the significant impacts of electrolyte's viscosity, Barton et al. further improved the dimensionless relation by involving Schmidt number [22].

However, when the MD method is applied, there must be a sharp drop in the experimentally obtained polarization curves to guarantee the depletion of the reactant on the carbon fiber surfaces in the limiting half cell [17]. Especially for certain sluggish redox reaction such as Cr^{2+}/Cr^{3+} and VO_2^+/VO^{2+} redox, the polarization curves are linear ones without sharp drops even though at relatively low flow rates, i.e., controlled by both mass transfer and kinetics [23,24,25]. To this concern, a polarization model is proposed in the present study that considers both the mass transfer and the electrochemical effects, termed as electrochemical-mass transfer jointly dominant polarization method (EMD method), to quantify how changes in electrode morphology and functional groups affect the mass transfer coefficient of the vanadium RFB.

The rest of the paper is organized as follows. First, the detailed mass transfer coefficient fitting model and related experimental setups are elaborated in Section 2 and Section 3, respectively. Then, the characterization of the electrode materials after varying pretreatments and the resulting polarization curves are compared vis-à-vis in Section 4. Last, the limitations of the EMD method and the future work for further improvement are presented in Section 5. Section 6 concludes the paper.

2. Model theory

In the present study, the mass transfer coefficient investigation is conducted based on the positive half-cell of the vanadium RFB. The chemical reaction in the positive side is:

$$VO^{2+} + H_2O \underset{\text{discharging}}{\overset{\text{charging}}{\rightleftarrows}} VO_2^+ + 2H^+ + e^- \tag{1}$$

During the charging or discharging of the flow cell, the current-overpotential relations of the positive or negative half-cell could be described by Butler-Volmer equation as:

$$i = i_0\left[\frac{c_o^s}{c_o}\exp\left(-\frac{\alpha n\mathrm{F}}{\mathrm{R}T}\eta\right) - \frac{c_r^s}{c_r}\exp\left(\frac{(1-\alpha)n\mathrm{F}}{\mathrm{R}T}\eta\right)\right] \tag{2}$$

$$i_0 = n\mathrm{F}ak_0 c_o^{1-\alpha} c_r^{\alpha} \tag{3}$$

$$\eta = E - E_{eq} \tag{4}$$

$$E = E_0 + \frac{\mathrm{R}T}{n\mathrm{F}}\ln\left(\frac{c_o}{c_r}\right) \tag{5}$$

where, i is the current density at the carbon fiber surface; i_0 is the exchange current density; α is the charge transfer coefficient; n is the number of the electrons transferred during the reaction; F is Faraday's constant; R is the gas constant; T is the temperature; a is the specific surface area of the electrode; k_0 is the reaction rate coefficient; c_o^s and c_r^s are the reactant concentrations at the carbon fiber surface ; c_o and c_r are the reactant concentrations in the bulk electrolyte; the subscripts o and r denote the oxidized and reduced species, respectively (in the present study, the oxidized and the reduced species refer to VO_2^+ and VO^{2+}, respectively); η is the overpotential; E is the half-cell potential during charging or discharging; E_{eq} is the equilibrium potential of the half-cell; and E_0 is the standard potential of the half-cell.

The current density at the surface of the carbon fibers in Butler-Volmer equation is proportional to the directional molar fluxes of the consumed reactant during the electrochemical reaction. Take the reduced reaction as example:

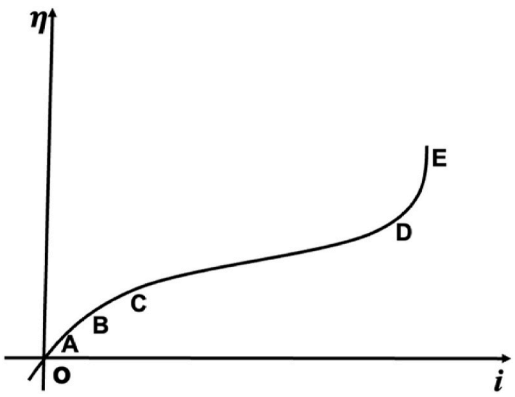

Fig. 1. Typical polarization curve (OA: linear polarization region; AB: weak polarization region; BC: Tafel region; CD: electrochemical-mass transfer dominant region; and DE: mass transfer dominant region).

$$i = n\mathrm{F}ak_m\left(c_o - c_o^S\right) \tag{6}$$

where, k_m denotes the mass transfer coefficient; and k_m (c_o-c_o^s), is the mass transfer rate of the consumed reactant guided by Fick's law.

When the concentration of the consumed reactant at the fiber surfaces reduces to zero, the resulting current density is the limiting current density as below:

$$i_l = n\mathrm{F}ak_m c_o \tag{7}$$

By considering Eqs. (6) and (7), the relation between the surface and bulk concentration of the consumed reactant can be derived:

$$\frac{c_o^s}{c_o} = 1 - \frac{i}{n\mathrm{F}ak_m c_o} \tag{8}$$

with the same process, the same relation for the reduced reactant can also be expressed as:

$$\frac{c_r^s}{c_r} = 1 - \frac{i}{n\mathrm{F}ak_m c_r} \tag{9}$$

Substituting Eqs. (8) and (9) into Eq. (2) relates the mass transfer coefficient to the Butler-Volmer model as:

$$i = i_0\left[\left(1 - \frac{i}{n\mathrm{F}ak_m c_o}\right)\exp\left(-\frac{\alpha n\mathrm{F}}{\mathrm{R}T}\eta\right) - \left(1 - \frac{i}{n\mathrm{F}ak_m c_r}\right)\exp\left(\frac{(1-\alpha)n\mathrm{F}}{\mathrm{R}T}\eta\right)\right] \tag{10}$$

when the overpotential value is relatively large ($\frac{e^{(1-\alpha)\frac{n\mathrm{F}}{\mathrm{R}T}\eta}}{e^{-\alpha\frac{n\mathrm{F}}{\mathrm{R}T}\eta}} = e^{\frac{n\mathrm{F}}{\mathrm{R}T}\eta} \le 0.01$, CD segment in Fig. 1), the effects of the reverse reaction (less than 1 %) could be ignored. Taking the reduction reaction as example, Eq. (10) can be further simplified as:

$$i = i_0\left[\left(1 - \frac{i}{n\mathrm{F}ak_m c_o}\right)\exp\left(-\frac{\alpha n\mathrm{F}}{\mathrm{R}T}\eta\right)\right] \tag{11}$$

Equation (11) can be further arranged as:

$$-\eta = \frac{\mathrm{R}T}{\alpha n\mathrm{F}}\ln\frac{i}{i_0} + \frac{\mathrm{R}T}{\alpha n\mathrm{F}}\ln\frac{n\mathrm{F}ak_m c_o}{n\mathrm{F}ak_m c_o - i} \tag{12}$$

in Eq. (12), the first and second terms on the right side refer to the reaction overpotential and the concentration overpotential, respectively. Thus, the mass transfer coefficient can be calculated by fitting the polarization data that satisfy $\frac{e^{(1-\alpha)\frac{n\mathrm{F}}{\mathrm{R}T}\eta}}{e^{-\alpha\frac{n\mathrm{F}}{\mathrm{R}T}\eta}} = e^{\frac{n\mathrm{F}}{\mathrm{R}T}\eta} \le 0.01$ (shown as the CD region in Fig. 1). The least squares method (based on the lsqcurvefit function) is adopted to fit multiple polarization data in one polarization curve to

Table 1
Labels for prepared electrode samples and corresponding pretreatments.

Label	Pretreatment processes
CF-P	Original carbon fiber bundles
CF-T200	Thermal treatment under 200 °C for 30 min
CF-T200 + R45	Thermal treatment under 200 °C for 30 min, and then reduction on Zn foil for 45 min
CF-T300	Thermal treatment under 300 °Cfor 30 min
CF-T300 + R45	Thermal treatment under 300 °C for 30 min, and then reduction on Zn foil for 45 min
CF-T400	Thermal treatment under 300 °C for 30 min
CF-T400 + R15	Thermal treatment under 400 °C for 30 min, and then reduction on Zn foil for 15 min
CF-T400 + R30	Thermal treatment under 400 °C for 30 min, and then reduction on Zn foil for 30 min
CF-T400 + R45	Thermal treatment under 400 °C for 30 min, and then reduction on Zn foil for 45 min

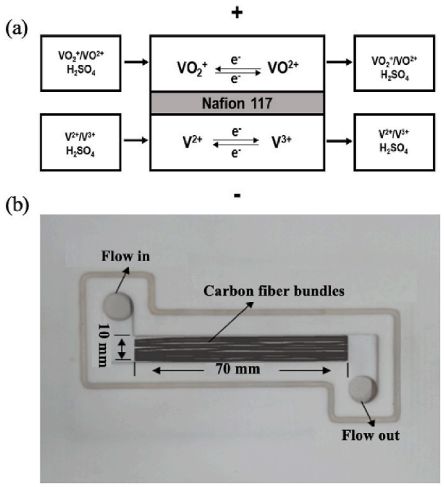

Fig. 2. (a) Schematic of four-tank vanadium redox flow cell; and (b) electrolyte flow frame and carbon fiber bundles in frame.

obtain the mass transfer coefficient.

When the overpotential of the flow cell is mainly dominated by the reaction loss (Tafel range, i.e., BC region in Fig. 1), the second term in Eq. (12) is further neglected, and thus the current-overpotential relation is further simplified as:

$$-\eta = \frac{RT}{\alpha n F}\ln\frac{i}{i_0} \tag{13}$$

Based on Eq. (13), a straight line taking lg(i) as the abscissa and η as the ordinate can be obtained. The intercept and slope refer to the exchange current density and the charge transfer coefficient of the reaction, respectively.

3. Experimental

3.1. Pretreatments and characterizations of electrode material

As the fiber alignment (pore microstructure) is complicated in the carbon felt or carbon paper electrodes, the carbon fiber bundles (SIGRAFIL® D 2–3 K) are used as the electrode material. The thermal treatment was first applied to the original bundles to alter the morphology and functional groups of the fiber surface. The thermal treatments were conducted under the air atmosphere for 30 min at 200 °C, 300 °C, or 400 °C for preparing multiple samples with varying morphologies and functional groups, respectively. Afterwards, to maintain the similar oxygen-containing functional groups in different thermally treated electrode samples, some samples were reduced on a high-purity Zn foil surface for 45 min. With such treatment, the oxygen-containing functional groups on the fiber surfaces were reduced without affecting the morphology. Besides, the electrode samples with the 400 °C thermal treatment were reduced with the Zn foil for 15, 30, or 45 min, respectively, to investigate the effects of different amounts of functional groups on the resulting mass transfer coefficient. The labels of the prepared samples are summarized in Table 1.

The scanning electron microscope (SEM) observations of morphologies on fiber surfaces were conducted by using a SU-70 field emission SEM. The X-ray photoelectron spectroscopy (XPS) surface analyses were performed to identify the amount of the functional groups on the surfaces by using Thermo Scientific ESCALAB 250Xi. The specific surface areas of the electrode samples were measured through the Brunauer-Emmett-Teller (BET) method with Autosorb-1-C to further verify the morphology change. Besides, the electrochemical double-layer capacitance (EDLC) was measured to derive the electrochemical accessible surface area of the electrode samples.

3.2. Electrochemical experiments

The four-tank flow cell is configurated to maintain a certain state-of-charge level at the inlet of the flow cell. As shown in Fig. 2a, both the positive and negative half-cells have two tanks, respectively. Thereby, the electrolyte did not go through cycles during the electrochemical experiments based on the four-tank setup. The electrolyte used was the vanadium-based electrolyte (1.6 M vanadium ions resolved in 4 M H_2SO_4). And the electrolytes were pumped from the positive and negative tanks to the cell through two peristaltic pumps (provided by the Masterflex Group). The Nafion® 117 was used to separate the positive and negative electrodes. The carbon fiber bundles were placed parallelly in the flow frame to be used as the positive and negative electrodes materials (see Fig. 2b). To enhance a uniform velocity distribution in the electrode, the electrolyte was guided by two parallel flow channels distributed between the inlet and the outlet. Besides, to guarantee the depletion of the reactant on the fiber surface in the limiting half cell, which was the positive half cell in the present study, the positive electrolyte was diluted to half of its original concentration by using the deionized water.

The polarization measurements of the flow cell with different electrode samples at varying flow rates (1 mL/min, 3 mL/min, 5 mL/min, or 8 mL/min) were conducted. The linear sweep voltammetry method (LSV) was adopted by scanning the potentials from the open circuit voltage to zero with the scanning rate corresponding to 10 mV/s. Besides, to determine the ohmic resistance of the flow cell, the electrochemical impedance measurements (EIS) were conducted. During the tests, the applied frequency varied from 10 mHz to 100 kHz, and the applied potential was set as the open circuit voltage. The iR-corrected polarization data were obtained accordingly. All the tests were proceeded on the Bio-Logic® VSP electrochemical workstation. In addition, the nitrogen protection was maintained for the flow cell to avoid the oxidation of the reactants, and the environmental temperature was controlled at 25 °C. Each test was conducted three times to ensure the repeatability of the testing results.

The EDLC specific surface area was measured through the Cyclic Voltammetry (CV) method (detailed results are provided in Supplementary Materials). To be noticed, the electrolyte was changed to the concentrated sulfuric acidic solution in the CV test to eliminate the effects of the faradaic current. The voltage varied from negative 0.3 V to positive 0.3 V with the scanning rates varying at 10 mV/s, 20 mV/s, 50 mV/s, 100 mV/s, and 200 mV/s. Based on the CV curves, the EDLC current is derived as:

$$I_{EDLC} = \frac{1}{2}(I_{ox} + |I_{red}|) \tag{14}$$

where, I_{ox} is the oxidized current, and I_{red} is the reduced current. The

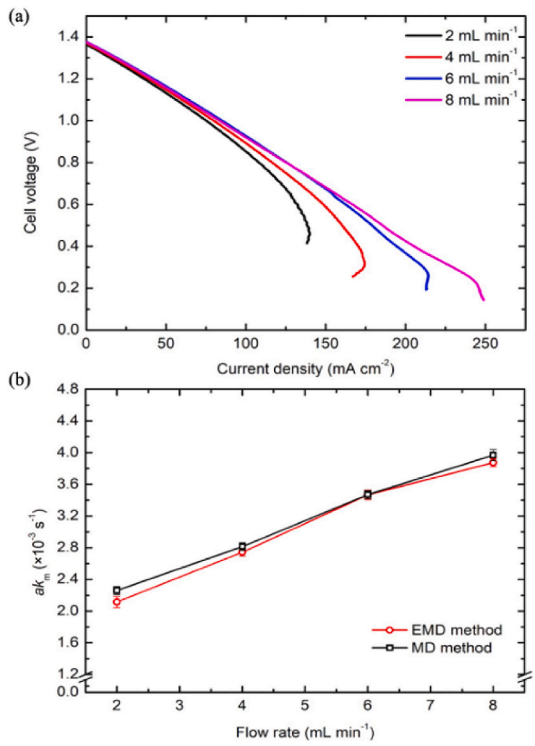

Fig. 3. (a) Experimental polarization curves; and (b) volumetric mass transfer coefficients obtained through EMD and MD methods based on experimental data.

EDLC, i.e., C_{EDLC}, is then calculated based on the EDLC current and the applied scanning rate:

$$C_{EDLC} = \frac{I_{EDLC}}{\nu} \tag{15}$$

where, ν is the scanning rate.

The EDLC specific surface area can be further derived:

$$a_{EDLC} = \frac{SC_{EDLC}}{C_{ref} m} a_{EDLC} = \frac{SC_{EDLC}}{C_{ref} m} \tag{16}$$

where, S is the electrode area; C_{ref} is the reference capacitance (23 μF/cm^2 in the present study); and m is the electrode quality.

4. Results and discussion

4.1. Validation of EMD method

The use of the MD method to determine mass transfer coefficients is highly recognized in the field of electrochemistry, and its effectiveness has been widely validated. Therefore, the mass transfer coefficients obtained by using the EMD approach are compared with those obtained by using the MD method in our work. Both the results are derived from the same sets of the polarization curves as shown in Fig. 3a (polarization data in the electrochemical-mass transfer jointly dominant region for the EMD method, and limiting current densities for the MD method). To be noticed, there exist inflection points in the ending area of the polarization curves in Fig. 3a, especially under low electrolyte flow rates. Based on our understanding, as the reactant mass transfer rate is substantially reduced under low flow rates, the mass transfer in the diffusion layer experiences an unsteady state. The premature state before the mass transfer in the electrode entering the completely steady state may lead to the inflection in the polarization curves. Nevertheless, the appearances of the inflection points have little effects on the limiting current densities which are determined according to the sharp reduction points in the curves. As Fig. 3b shows, there are good agreements between the volumetric mass transfer coefficients obtained through the MD and EMD methods, respectively. The deviations are within 7 %, which are possibly due to the fitting data selection bias, especially for the MD method. It should be noted that while the similarity in results between EMD and MD methods may not indicate a significant difference in this specific instance, it still holds value in terms of method validation in our research. This is a critical guarantee for the reliability of subsequent

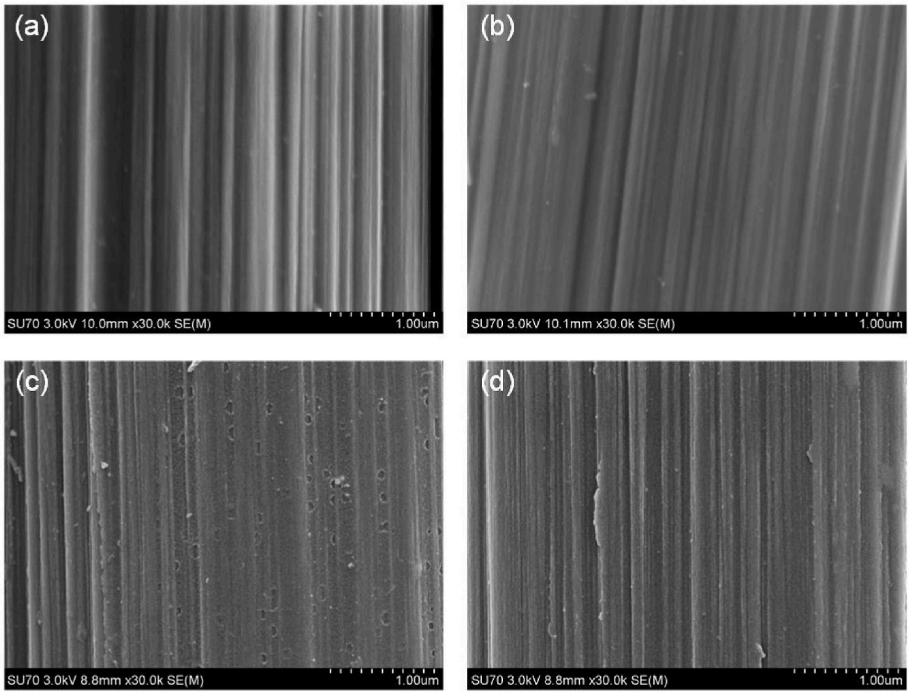

Fig. 4. SEM images of carbon fiber surfaces: (a) original carbon fiber; (b) fiber thermally treated under 200 °C for 30 min; (c) fiber thermally treated under 300 °C for 30 min; and (d) fiber thermally treated under 400 °C for 30 min.

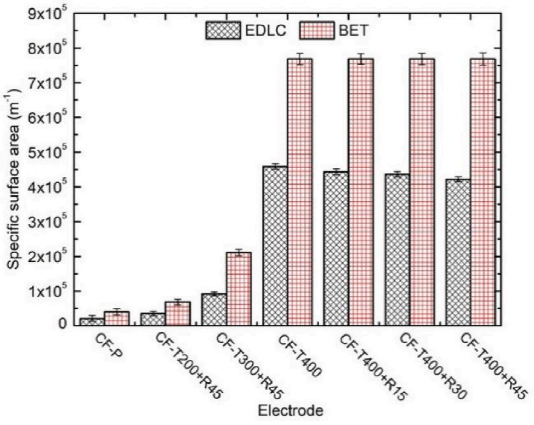

Fig. 5. Specific surface area results of different carbon fiber bundles obtained through BET and EDLC methods. Please refer to Table 1 for sample labels.

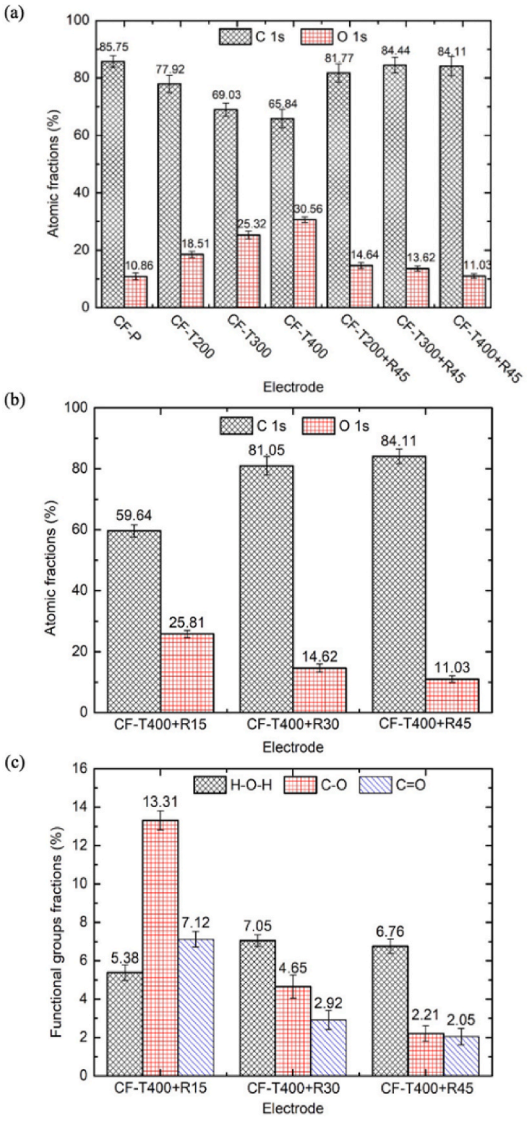

Fig. 6. XPS results: (a) O/C atomic ratios on carbon fiber surfaces with varying pretreatments; (b) O/C atomic ratios on carbon fiber surfaces with 400 °C thermal treatment and varying reduction durations; (c) oxygen-containing functional groups fraction of carbon fiber surfaces with 400 °C thermal treatment and varying reduction durations. Please refer to Table 1 for sample labels.

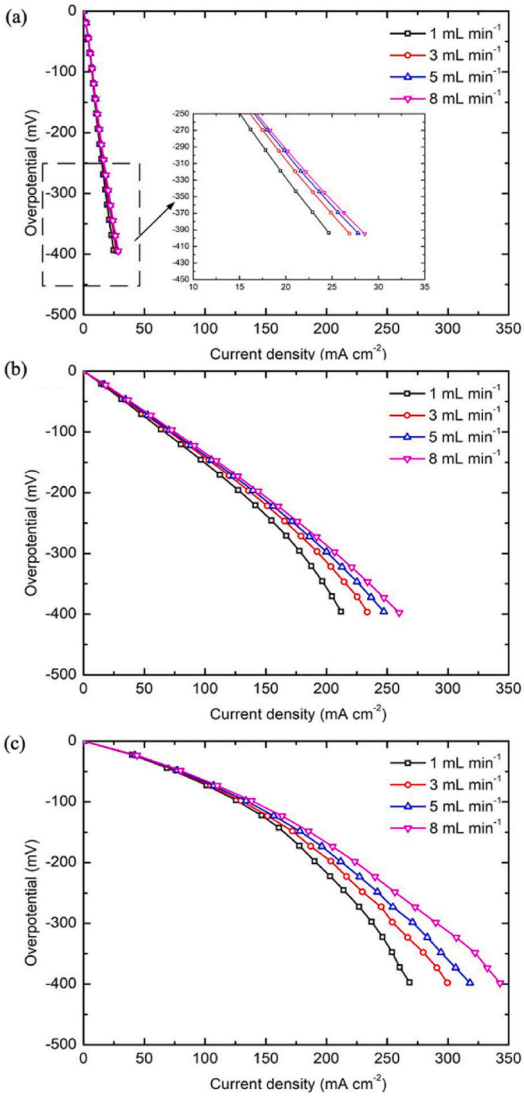

Fig. 7. Polarization curves of flow cells with different carbon fiber bundles as electrodes: (a) samples under 200 °C thermal treatment; (b) samples under 300 °C thermal treatment; and (c) samples with 400 °C thermal treatment. Samples undergo a 45-min Zn foil reduction pretreatment.

research results. In summary, using the EMD method to fit the mass transfer coefficient has high reliability, and the experimental data used is easy to obtain, particularly for linear polarization curves (e.g., Fig. 7). Therefore, all subsequent studies in the following subsections are carried out by using the EMD method.

4.2. Morphology, specific surface area, and functional groups

The surface morphologies of carbon fibers before and after the thermal pretreatments are captured through SEM. As shown in Fig. 4a, the surface of the original carbon fiber is smooth and exists undulating stripes. After the thermal treatments at different temperatures, the surface morphologies change in different ways. First, the thermal treatment at 200 °C for 30 min does not significantly change the surface morphology (Fig. 4b). As the temperature increases to 300 °C, the surface becomes rough obviously, and the observable pores appear (Fig. 4c). With the temperature further increasing to 400 °C, the fiber surface is still rough with pores on the surface disappearing (Fig. 4d), which transform into smaller, denser nanoscale voids (similar phenomenon was also observed in previous studies [26]). The BET method is used to further quantify the specific surface areas of the carbon fiber

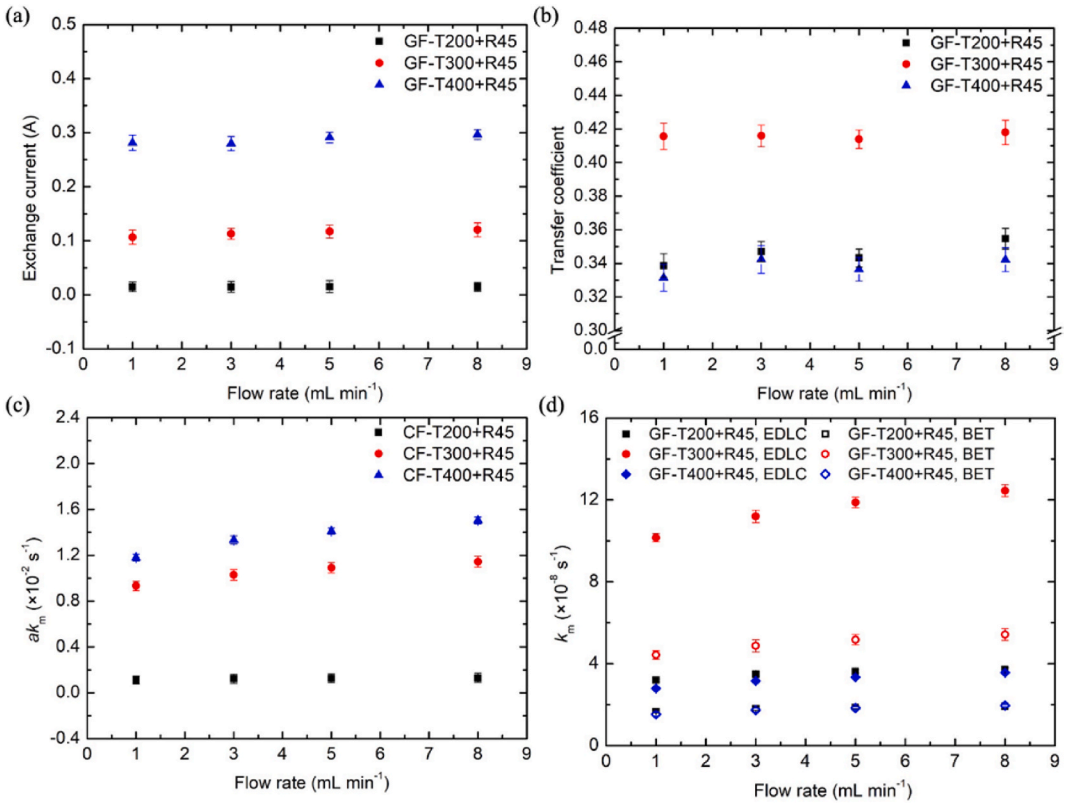

Fig. 8. Model fitting results of flow cells with different carbon fiber bundles as electrodes through EMD method: (a) exchange current; (b) charge transfer coefficient; (c) volumetric mass transfer coefficient; and (d) mass transfer coefficient. Please refer to Table 1 for sample labels. Samples undergo a 45-min Zn foil reduction pretreatment.

bundles under different pretreatments, and the results are shown in Fig. 5. The specific surface area increases with the rising treatment temperatures: The specific surface area of the bundles with the thermal treatment under 400 °Cis approximately 19 times of the specific surface area of the original sample. Besides, the specific surface area values show no apparent differences in the samples with and without the Zn foil reduction pretreatment (400 °C thermal treatment). To evaluate the specific surface area that takes part into the electrochemical reaction, the EDLC method is also adopted. As Fig. 5 shows, the electrochemical specific surface area is approximately half of the BET results, possibly owing to that the electrolyte can not reach some of the small-scale pores observed on the fiber surfaces. Besides, the electrochemical specific surface area decreases slightly when the Zn foil reduction (400 °C thermal treatment) is applied and with the increasing reduction duration. The reduction in the electrochemical specific surface area may be associated with the reduction in the oxygen-containing functional groups which contribute to the electrode hydrophilicity.

With different pretreatments, the corresponding atomic ratio of the oxygen to the carbon (O/C) and the amounts of different oxygen-containing functional groups on the fiber surfaces also change. For the samples that undergo thermal treatment without the Zn foil reduction, the O atomic fraction increases with the rising treatment temperature (Fig. 6a). While when the 45-min reduction is applied on above samples, the O/C ratios of different samples are reduced to the similar values, showing that the variations in the O/C ratio, along with the relevant effects on the mass transfer coefficient, resulting from the rising treatment temperature are effectively recovered when the Zn foil reduction treatment lasts for 45 min. Besides, the O/C atomic ratios and the functional groups of the samples with 400 °C thermal treatment and different reduction durations are shown in Fig. 6b and c. As the result shows, the atomic oxygen ratio decreases as the reduction duration increases from 15 min to 45 min (Fig. 6b), resulting from the reduced C–O and C═O functional groups (Fig. 6c). Therefore, the samples under 400 °C thermal treatment and varying durations of the reduction treatment are prepared to investigate the effects of the variations in the oxygen-containing functional groups on the mass transfer coefficient.

4.3. *Effects of morphology on mass transfer coefficient*

To investigate the effects of the surface morphology on the mass transfer coefficient, the samples were pretreated at different temperatures (corresponding changes in the fiber surface morphology are shown in Fig. 4) and undergone the 45-min reduction treatment to maintain the similar C/O ratio on the surface (Fig. 6a) before the polarization measurements. As shown in Fig. 7, for all the investigated samples (CF-T200 + R45, CF-T300 + R45, and CF-T400 + R45), the increased flow rates decrease the overpotential. The mass transfer coefficients are fitted by using the EMD method which enables the estimation for the mass transfer coefficient by using the data in the electrochemical-mass transfer jointly dominant polarization region, and the fitting results are shown in Fig. 8.

The exchange current and the charge transfer coefficient are also fitted out (Eq. (13)) according to the polarization curves in Fig. 7. As shown in Fig. 8a and b, the change in the flow rate has minor effects on these two parameters which are dependent on the electrochemical kinetics rather than the mass transfer of ions in the electrolyte. With respect to the exchange current, it increases with the increasing thermal treatment temperature owing to the increments in the specific surface area. By contrast, the charge transfer coefficient is related to the characteristics of the interface between the electrolyte and the electrode. Thereby, the fitted charge transfer do not exhibit meaningful trends with the increasing treatment temperatures, and the values are in the range of 0.32–0.42, which are consistent with literature values (0.2–0.9) [27,28].

Based on the exchange current and the charge transfer coefficient,

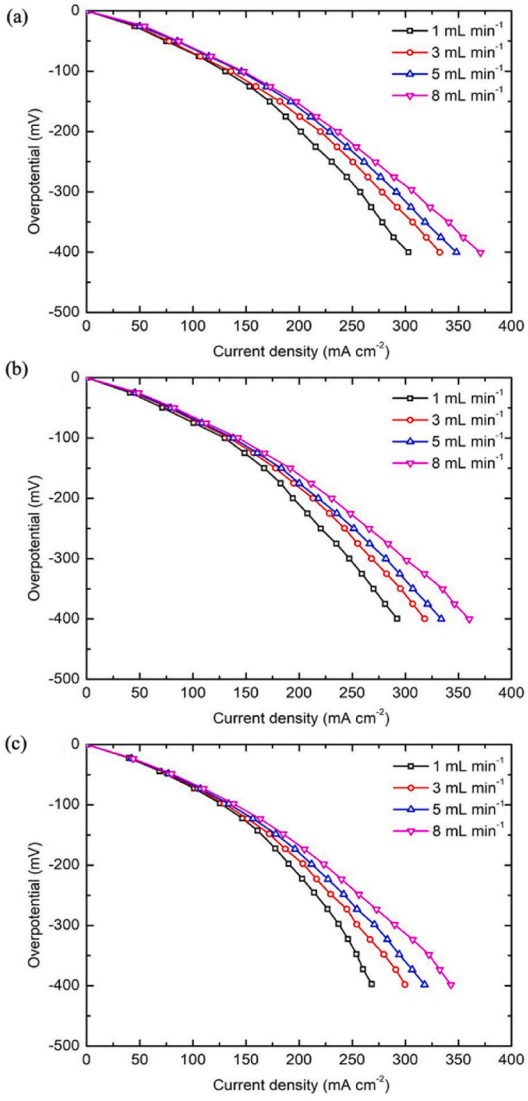

Fig. 9. Polarization curves of flow cells with different carbon fiber bundles as electrodes: (a) samples under 400 °C thermal treatment and 15-min reduction treatment; (b) samples under 400 °C thermal treatment and 30-min reduction treatment; and (c) samples under 400 °C thermal treatment and 45-min reduction treatment.

the mass transfer coefficient is further fitted out (see Section 2; here, the MD method cannot be used because there are no sharp drops in the polarization curves). As shown in Fig. 8c, the volumetric mass transfer coefficients (defined as the mass transfer coefficient multiplying the specific surface area of the electrode) increase with the rising thermal treatment temperatures, showing that the morphology changes on the fiber surfaces are beneficial for the volumetric mass transfer coefficient in the electrode. This may result from the enhanced concentration gradient of the reactants from the bulk electrolyte toward the fiber surface, as the enlarged specific surface area decreases the concentration on the surface. To further eliminate the effects of the specific surface area, the mass transfer coefficients are also calculated based on the specific surface areas derived from the EDLC method and the BET method (Fig. 5). As shown in Fig. 8d, due to the distinct morphologies resulting from the pretreatments at different temperatures, the mass transfer coefficients also display distinct variations. The pores and roughness appeared on the fiber surfaces when the 300 °C thermal treatment is applied are shown to effectively enhance the mass transfer process of the reactants in the electrode (Fig. 4c), which is consistent with the observations in the literature [29]. Nevertheless, the nano-scale pores on the surface, though significantly enhance the EDLC and the BET specific surface areas, showing insignificant effects on the mass transfer enhancement within the diffusion layer. It can be inferred that if the limiting current region can be reached in the polarization curves (such as through reduction in the reactant concentration or the flow rate, which may lead to unstable polarization curves though), similar limiting current densities would be observed for the GF-T200 + R45 and the GF-T400 + R45 samples. It brings an important research question that how to optimize the surface morphology of the fibers to make a balance between the specific surface area and the mass transfer capability. Some previous studies have proposed dual-scale pores for addressing this challenge [29]. Nevertheless, further studies should be conducted to lay a deep understanding on the fundamentals regarding the impacts of the surface morphology on the mass transfer.

It is worth noting that there are some deviations in the fitting results. The deviations are largely related to the uncertainty of the testing instrument and also the simplification assumptions made in the fitting model (see in Section 2). However, as shown in the figure, the relevant deviations are within an acceptable range and do not affect the relevant conclusions.

4.4. *Effects of functional groups on mass transfer coefficient*

The samples with the 400 °C thermal treatment were reduced by using the Zn foil for varying durations to prepare comparative cases with the similar surface morphology but distinct functional groups (Fig. 6). As shown in Fig. 9, the overpotentials of the flow cell slightly increase with the longer reduction, owing to the reduction in the oxygen-containing functional groups. Nevertheless, the impacts on the polarization performance are limited.

As shown in Fig. 10a, the exchange current increases when the reduction duration is shorten, as the improved oxygen containing functional groups are beneficial for the reaction kinetics. For the charge transfer coefficient, the fitted values span the range of 0.33–0.36 (Fig. 10b). The corresponding mass transfer coefficients are all improved with the increasing amount of the oxygen-containing functional groups which yield better hydrophilicity of the electrode. Last but not least, to extend the experimental results presented here to other flow systems, the mass transfer coefficients are generalized by establishing the correlations between the dimensionless parameters Sh ($Sh = \frac{k_m d}{D}$, d is the carbon fiber diameter, and D is the diffusivity of the redox-active species) and Re ($Re = \frac{ud}{\nu}$, u is the electrolyte velocity in porous electrode, and ν is the electrolyte kinematic viscosity) by using the least square fitting method (results see Fig. 11). As the results show, the selection of the specific surface area value does not affect the power value in the correlations. Besides, compared with the effects of the oxygen-containing functional groups (Fig. 11b), the influence of the morphology changes (Fig. 11a) on the correlations is more significant, owing to its effects on the diffusion layer velocity and the concentration distribution.

5. Limitations and future work

Although the results indicate that both the surface morphology and the functional groups impact the mass transfer of reactants in the diffusion layer, there are a few further improvements that should be examined in the future work. First, the investigations on the essential mechanisms of the functional groups should be further conducted. For example, how does the hydrophilicity specifically affect the capillary force and the saturation of the electrolyte [30,31]. In addition, the impacts of the microstructure of the electrode on the reactant mass transfer is inadequately understood (particulary for novel materials such as layered double hydroxides array modification [35]). Additionally, further studies should be conducted to address the fundamentals regarding the impacts of the surface morphology on the mass transfer.

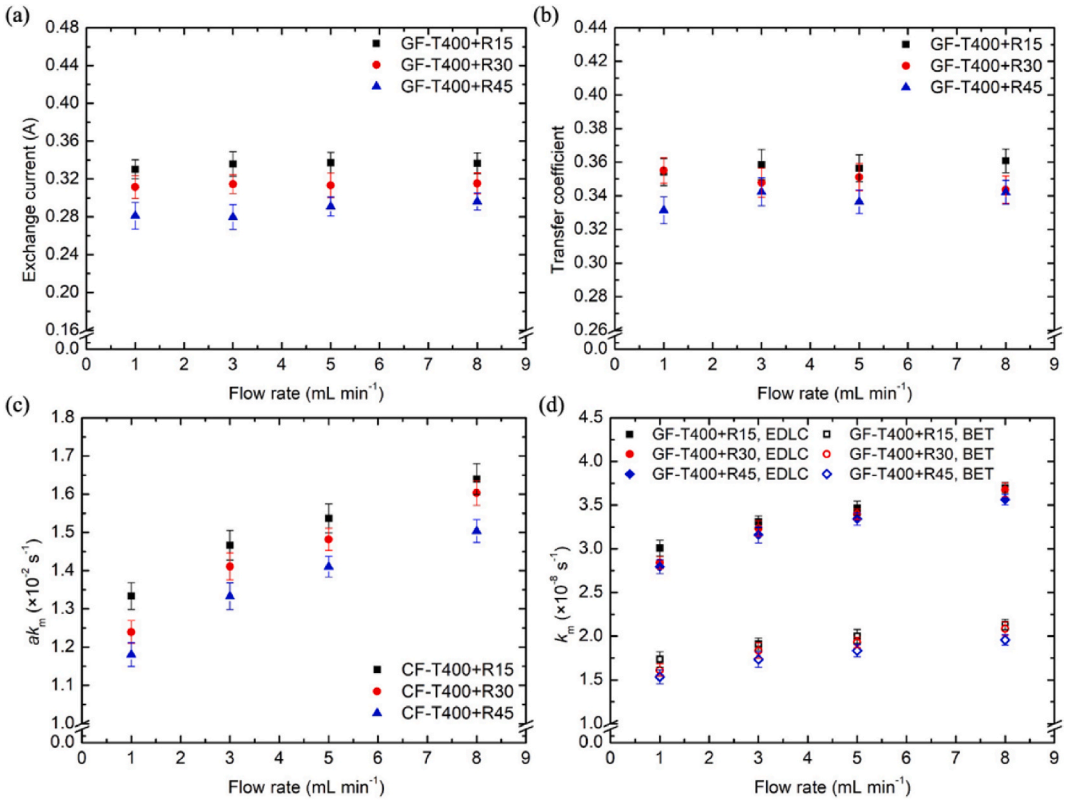

Fig. 10. Model fitting results of flow cells with different carbon fiber bundles as electrodes through EMD method: (a) exchange current; (b) charge transfer coefficient; (c) volumetric mass transfer coefficient; and (d) mass transfer coefficient. Please refer to Table 1 for sample labels.

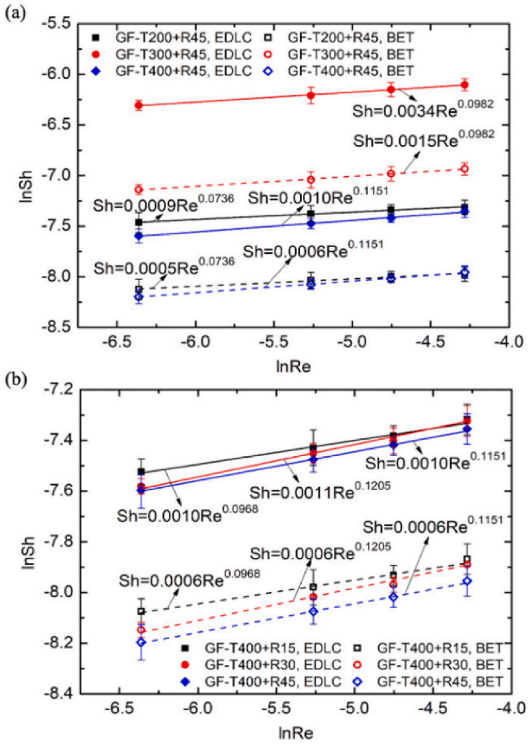

Fig. 11. Dimensionless equations of the mass transfer coefficients: (a) samples under thermal treatments at different temperatures and 45-min reduction treatment; (b) samples under 400 °C thermal treatment and different reduction durations. Please refer to Table 1 for sample labels.

With above mentioned deep understandings, the size and the shape of the pores appeared on the carbon fiber surfaces will be optimized and well controlled by using advanced manufacturing technologies in the future. Besides, the experiments in the present study are conducted on the VRFB cell at the lab scale. Further experiments should be conducted on the large-scale flow cells to verify the related conclusions. Last, although the present study focuses on carbon fibers, the emerging materials for novel systems such as reduced graphene oxide and vertically oriented graphene should also be paid attention to in the future's work [32–34].

6. Conclusions

The present study explored the mechanism of how changes in electrode morphology and functional groups affect the mass transfer coefficient, through controlled thermal treatment that changes the surface morphology and zinc reduction treatment that alters the oxygen-containing functional groups on the fiber surface. And the developed fitting model considers both the mass transfer and the electrochemical effects, enabling efficient mass transfer coefficient characterization for redox flow battery systems with sluggish reactants (i.e., polarization curve exhibits a linear trend).

Main findings of the present study are as follows.

(i) The volumetric mass transfer coefficient of the electrode increased when the carbon fibers were thermally treated. Further, when the specific surface areas were eliminated, resulting pores at different scales on the carbon fiber surfaces, which were generated by the thermal treatment at different temperatures, affected the mass transfer coefficient of the flow cell in opposite ways. In general, the micro-scale pores on the fiber surface, when fibers were thermally treated at 300 °C, successfully enhanced the mass transfer process of the reactants in the electrode likely

owing to the shortened diffusion distance, while the nano-scale pores, when fibers were thermally treated at 400 °C, showed minor effects on mass transfer enhancement.

(ii) The volumetric mass transfer coefficient and mass transfer coefficient both increased with the increasing amount of the oxygen-containing functional groups, which was likely due to that the improved electrode hydrophilicity was preferable by the mass transfer process of the reactants in the electrode.

Regarding the practical implication, the findings of the present work suggest balancing the distinct effects of micro-scale and nano-scale pores on the fiber surface to simultaneously enhance the mass transfer within the diffusion layer and specific surface area. In particular, the mass transfer enhancement is expected through the introduction of micro-scale pores and oxygen-containing functional groups, similar with those formed when the carbon fibers were thermally treated at 400 °C. Last but not least, the developed mass transfer coefficient characterization method enables the efficient and accurate measurement of the mass transfer coefficient in RFBs for sluggish redox such as Cr^{2+}/Cr^{3+} and VO_2^+/VO^{2+} redox, which is critical for the success of simulative studies. The main findings of the present study are also expected to enable frontend screening in future's electrode development campaigns by establishing the power-law correlations for Sherwood number and Reynolds number for different electrode samples (see Fig. 11).

CRediT authorship contribution statement

Menglian Zheng: Conceptualization, Formal analysis, Funding acquisition, Investigation, Methodology, Validation, Writing – original draft, Writing – review & editing. **Ke Liu:** Investigation, Methodology, Validation, Visualization, Formal analysis. **Jie Sun:** Investigation, Validation, Writing – original draft. **Zitao Yu:** Methodology, Supervision.

Declaration of competing interest

The authors declare the following financial interests/personal relationships which may be considered as potential competing interests:

Menglian Zheng reports was provided by Fundamental Research Funds for the Central Universities. Jie Sun reports was provided by Zhejiang Provincial Natural Science Foundation of China. Menglian Zheng reports was provided by National Natural Science Foundation of China. If there are other authors, they declare that they have no known competing financial interests or personal relationships that could have appeared to influence the work reported in this paper.

Data availability

Data will be made available on request.

Acknowledgements

This work was supported by the Fundamental Research Funds for the Central Universities [grant number 2022ZFJH004], the Zhejiang Provincial Natural Science Foundation of China [grant number LQ23E060003], and the National Natural Science Foundation of China [grant number 51606164], Ningbo Municipal Natural Science Foundation of China [grant number 2023J398].

Appendix A. Supplementary data

Supplementary data to this article can be found online at https://doi.org/10.1016/j.energy.2024.130237.

References

[1] Olabi AG, Onumaegbu C, Wilberforce T, et al. Critical review of energy storage systems. Energy 2021;214:118987.
[2] Park M, Ryu J, Wang W, et al. Material design and engineering of next-generation flow-battery technologies. Nat Rev Mater 2017;2(1):16080.
[3] Li Z, Lu YC. Material design of aqueous redox flow batteries: fundamental challenges and mitigation strategies. Adv Mater 2020;32(47):2002132.
[4] Kumar R, Sahoo S, Joanni E, et al. Recent progress in the synthesis of graphene and derived materials for next generation electrodes of high performance lithium ion batteries. Prog Energy Combust Sci 2019;75:100786.
[5] Sahoo S, Kumar R, Joanni E, et al. Advances in pseudocapacitive and battery-like electrode materials for high performance supercapacitors. J Mater Chem A 2022;10(25):13190–240.
[6] Zheng M, Sun J, Meinrenken CJ, et al. Pathways toward enhanced techno-economic performance of flow battery systems in energy system applications. Journal of Electrochemical Energy Conversion and Storage 2019;16(2):021001.
[7] Zhang J, Yang H, Huang Z, et al. Pore-structure regulation and heteroatom doping of activated carbon for supercapacitors with excellent rate performance and power density. Waste Dispos Sustain Energy 2023;5:417–26.
[8] He Z, Lv Y, Zhang T, et al. Electrode materials for vanadium redox flow batteries: intrinsic treatment and introducing catalyst. Chem Eng J 2022;427:131680.
[9] Zhou XL, Zeng YK, Zhu XB, et al. A high-performance dual-scale porous electrode for vanadium redox flow batteries. J Power Sources 2016;325:329–36.
[10] Fu H, Bao X, He M, et al. Defect-rich graphene skin modified carbon felt as a highly enhanced electrode for vanadium redox flow batteries. J Power Sources 2023;556:232443.
[11] Abbas S, Lee H, Hwang J, et al. A novel approach for forming carbon nanorods on the surface of carbon felt electrode by catalytic etching for high-performance vanadium redox flow battery. Carbon 2018;128:31–7.
[12] Li W, Liu J, Yan C. Multi-walled carbon nanotubes used as an electrode reaction catalyst for VO2+/VO2+ for a vanadium redox flow battery. Carbon 2011;49(11):3463–70.
[13] Storck A, Robertson PM, Ibl N. Mass transfer study of three-dimensional electrodes composed of stacks of nets. Electrochim Acta 1979;24(4):373–80.
[14] Fedkiw PS, Newman J. Mass-transfer coefficients in packed beds at very low Reynolds numbers. Int J Heat Mass Tran 1982;25(7):935–43.
[15] Schmal D, Erkel JV, Duin P. Mass transfer at carbon fibre electrodes. J Appl Electrochem 1986;16(3):422–30.
[16] You X, Ye Q, Cheng P. The dependence of mass transfer coefficient on the electrolyte velocity in carbon felt electrodes: determination and validation. J Electrochem Soc 2017;164(11):E3386.
[17] Xu Q, Zhao TS. Determination of the mass-transport properties of vanadium ions through the porous electrodes of vanadium redox flow batteries. Phys Chem Chem Phys 2013;15(26):10841–8.
[18] Sun J, Zheng M, Luo Y, et al. Three-dimensional detached serpentine flow field design for redox flow batteries. J Power Sources 2019;428:136–45.
[19] Milshtein JD, Tenny KM, Barton JL, et al. Quantifying mass transfer rates in redox flow batteries. J Electrochem Soc 2017;164(11):E3265.
[20] Forner-Cuenca A, Penn EE, Oliveira AM, et al. Exploring the role of electrode microstructure on the performance of non-aqueous redox flow batteries. J Electrochem Soc 2019;166(10):A2230–41.
[21] Tenny KM, Forner-Cuenca A, Chiang Y, et al. Comparing physical and electrochemical properties of different weave patterns for carbon cloth electrodes in redox flow batteries. Journal of Electrochemical Energy Conversion and Storage 2020;17:041108.
[22] Barton JL, Milshtein JD, Hinricher JJ, et al. Quantifying the impact of viscosity on mass-transfer coefficients in redox flow batteries. J Power Sources 2018;399:133–43.
[23] Ahn Y, Moon J, Park SE, et al. High-performance bifunctional electrocatalyst for iron-chromium redox flow batteries. Chem Eng J 2021;421:127855.
[24] Aaron D, Tang Z, Papandrew AB, et al. Polarization curve analysis of all-vanadium redox flow batteries. J Appl Electrochem 2011;41:1175–82.
[25] Kok MDR, Jervis R, Tranter TG, et al. Mass transfer in fibrous media with varying anisotropy for flow battery electrodes: direct numerical simulations with 3D X-ray computed tomography. Chem Eng Sci 2019;196:104–15.
[26] Vudis PK, Jayanti S, Chetty R. State of charge and power rating gains in industrial-scale vanadium redox flow batteries through thermal activation of electrodes. J Energy Storage 2023;72:108734.
[27] Okedi TI, Fisher AC, Yunus K. Quantitative analysis of the effects of morphological changes on extracellular electron transfer rates in cyanobacteria. Biotechnol Biofuels 2020;13:1–14.
[28] Arvand M, Gholizadeh TM. Gold nanorods–graphene oxide nanocomposite incorporated carbon nanotube paste modified glassy carbon electrode for voltammetric determination of indomethacin. Sensor Actuator B Chem 2013;186:622–32.
[29] Wang R, Li YS, He YL. Achieving gradient−pore−oriented graphite felt for vanadium redox flow batteries: meeting improved electrochemical activity and enhanced mass transport from nano to micro scale. J Mater Chem A 2019;7:10962–70.
[30] Wang YB, Wang YF, Gao SR, et al. Universal model for the maximum spreading factor of impacting nanodroplets: from hydrophilic to hydrophobic surfaces. Langmuir 2020;36(31):9306–16.
[31] Wang YF, Wang YB, Xie FF, et al. Spreading and retraction kinetics for impact of nanodroplets on hydrophobic surfaces. Phys Fluids 2020;32(9).

[32] Tan WK, Asami K, Maegawa K, et al. Fe3O4-embedded rGO composites as anode for rechargeable FeOx-air batteries. Mater Today Commun 2020;25:101540.
[33] Kumar R, Singh RK, Alafcedov AV, et al. Rapid and controllable synthesis of Fe3O4 octahedral nanocrystals embedded-reduced graphene oxide using microwave irradiation for high performance lithium-ion batteries. Electrochim Acta 2018;281:78–87.
[34] Kuang W, Yang H, Ying C, et al. Cost-effective, environmentally-sustainable and scale-up synthesis of vertically oriented graphenes from waste oil and its supercapacitor applications. Waste Dispos Sustain Energy 2021;3:31–9.
[35] Wang P, Zhang K, Li H, et al. Enhanced ion transport through mesopores engineering with additional adsorption of layered double hydroxides array in alkaline flow batteries. Small 2023:2308791.